Available online at www.sciencedirect.com
ScienceDirect
Journal of Solid State Chemistry 180 (2007) 549–557
JOURNAL OF SOLID STATE CHEMISTRY
www.elsevier.com/locate/jssc

# The local crystal chemistry and dielectric properties of the cubic pyrochlore phase in the $Bi_2O_3$–$M^{2+}O$–$Nb_2O_5$ ($M^{2+}$ = $Ni^{2+}$ and $Mg^{2+}$) systems

Binh Nguyen, Yun Liu, Ray L. Withers*

*Research School of Chemistry, Australian National University, Canberra, ACT 0200, Australia*

Received 12 September 2006; received in revised form 25 October 2006; accepted 25 October 2006
Available online 17 November 2006

**Abstract**

The composition, dielectric properties and inherent displacive disorder of a Bi-based, misplaced-displacive cubic pyrochlore phase found in two ternary $Bi_2O_3$–$M^{2+}O$–$Nb_2O_5$ ($M$ = Ni and Mg) systems has been investigated. The dielectric permittivities (up to 1 MHz) of $(Bi_{0.825}Ni_{0.125}\square_{0.05})_2(Ni_{0.25}Nb_{0.75})_2O_7$ and $(Bi_{0.835}Mg_{0.085}\square_{0.08})_2(Mg_{0.235}Nb_{0.765})_2O_7$ at room temperature are found to be 116 and 151, respectively, while the dielectric loss tangents are 0.00065 and 0.00042, respectively, at 100 kHz. A highly structured characteristic diffuse intensity distribution apparent in electron diffraction is reported in both cases and partially interpreted in terms of large amplitude, $\beta$-cristobalite-type tetrahedral rotations of the O'$A_2$ tetrahedral framework sub-structure of the ideal pyrochlore structure type. Bond valence sum calculations are used to investigate the local crystal chemistry responsible for this displacive disorder.


*Keywords:* Misplaced-displacive cubic pyrochlores

## 1. Introduction

A displacively disordered, Bi-based pyrochlore phase found in a range of ternary $Bi_2O_3$–$M^{2+}O$–$Nb_2O_5$ systems [1–3] has been the subject of much recent interest as a result of its relatively low sintering temperatures and often excellent dielectric properties [1,2,4–6], including electric field tuneability [6]. The composition of the phase was initially assumed to be fixed and of ideal/'sensible' stoichiometry $Bi_2(M^{2+}_{2/3}Nb^{5+}_{4/3})O_7$ [1]. Recent careful phase analysis studies, however, have shown that the cubic pyrochlore phase in such systems is often a solid solution, invariably significantly Bi-deficient with respect to the above ideal stoichiometry and requires the presence of nominally too small $M^{2+}$ cations on the $A$ as well as the $B$ sites of the ideal $A_2B_2O_7$ pyrochlore structure type (see Fig. 1) [7–9]. They have thus been christened "… misplaced-displacive cubic pyrochlore …" phases [7]. The local crystal chemistry underlying such behaviour is still far from understood [7,10,11].

The archetypal such phase is $(Bi_{1.5}Zn_{0.5-\delta})(Zn_{0.5}Nb_{1.5})O_{7-\delta}$ (BZN) [2–7,10,11]. Its relatively high dielectric constant, low dielectric loss as well as compositionally tuneable temperature coefficient of capacitance (when used in conjunction with a nearby monoclinic zirconolite-like $Bi_2(Zn^{2+}_{2/3}Nb^{5+}_{4/3})O_7$ ternary phase within the $Bi_2O_3$–$Zn^{2+}O$–$Nb_2O_5$ system [2,4,7,9,10]) makes this material very attractive for low fire, high frequency multi-layer device applications [1,2,4–6]. To date, there have still been relatively few investigations of the effect of cation substitution upon the dielectric properties of BZN [12–15] or studies of the related $(Bi_{1.5}M^{2+}_{0.5-\delta})(M^{2+}_{0.5}Nb_{1.5})O_{7-\delta}$ materials [1,3,8].

Cann et al. [1] reported the synthesis and dielectric properties of nominally $Bi_2(M^{2+}_{2/3}Nb^{5+}_{4/3})O_7$, $M$ = Zn, Ni and Mg, cubic pyrochlores and Sirotinkin and Bush [3] those of nominally $(Bi_{1.5}M^{2+}_{0.5})(M^{2+}_{0.5}Nb^{5+}_{1.5})O_7$, $M$ = Zn, Ni, Mg, Cu and Mn, cubic pyrochlores. Their results, however, are not in good agreement as regards either composition or dielectric properties for both the $M$ = Ni and Mg

*Corresponding author. Fax: +61 2 6125 0750.
*E-mail address:* withers@rsc.anu.edu.au (R.L. Withers).

0022-4596/$ - see front matter © 2006 Elsevier Inc. All rights reserved.
doi:10.1016/j.jssc.2006.10.039

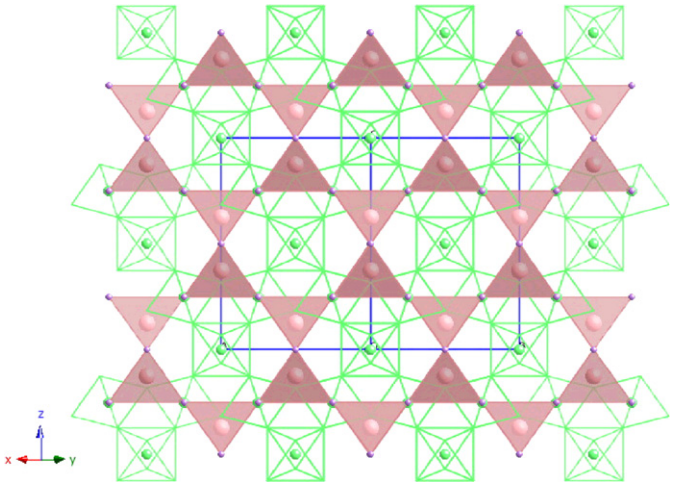

Fig. 1. The ideal pyrochlore $A_2B_2O_7$ or $B_2O_6.O'A_2$ structure type projected along a ⟨110⟩direction. The $B_2O_6$ octahedral framework sub-structure is represented by the open octahedra while the O'$A_2$ tetrahedral framework sub-structure is represented by the solid tetrahedra. The unit cell is shown in projection.

compounds, or indeed for BZN itself. In the case of the $M$ = Ni phase, for example, Cann et al. [1] report a room temperature dielectric constant for $Bi_2(Ni^{2+}_{2/3}Nb^{5+}_{4/3})O_7$ of 122 (at 1 MHz) while Sirotinkin and Bush [3] report a dielectric constant for $(Bi_{1.5}\ M^{2+}_{0.5})(M^{2+}_{0.5}Nb^{5+}_{1.5})O_7$ of only ~27 (at 10 kHz). As regards the disagreement in composition, Valant and Suvorov [16] have very recently carried out a detailed phase analysis investigation of the $Bi_2O_3$–NiO–$Nb_2O_5$ system. They report the existence of a non-stoichiometric (although quite compact) cubic pyrochlore solid solution with a composition centred around $Bi_{1.5}Ni_{0.67}Nb_{1.33}O_{6.25}$ (or $Bi_{1.68}Ni_{0.75}Nb_{1.49}O_7$ if normalized to seven oxygens) rather than the $Bi_2(Ni_{2/3}Nb_{4/3})O_7$ composition assumed by Cann et al. [1] or the $(Bi_{1.5}M^{2+}_{0.5})(M^{2+}_{0.5}Nb^{5+}_{1.5})O_7$ composition reported by Sirotinkin and Bush [3].

One purpose of the current paper is to re-investigate the composition and dielectric properties characteristic of the $M$ = Ni and Mg members of this family of cubic pyrochlore phases with a view to resolving some of the above apparent discrepancies. A further and equally important objective is to investigate the relationship between the local crystal chemistry of these cubic pyrochlore phases and inherent displacive disorder therein as manifested in the presence of heavy displacive disorder and resultant highly structured diffuse scattering [11,17,18].

## 2. Experimental

The initial syntheses assumed a nominal ideal composition for the cubic pyrochlore phase of $(Bi_{1.5}\ M^{2+}_{0.5})(M^{2+}_{0.5}Nb^{5+}_{1.5})O_7$ ($M$ = Ni and Mg), as assumed by Sirotinkin and Bush [3]. The starting materials used were highly pure $Bi_2O_3$, $Nb_2O_5$, NiO and MgO, respectively. The appropriate oxides were initially homogeneously mixed in acetone for 30 min using an agate mortar, then calcined at 850 °C for 1 day in a Pt crucible followed by regrinding in acetone for a further 30 min. They were then pressed into 1 cm diameter pellets and sintered at a higher temperature of 1050 °C for a further 1–3 days. The resultant pellets were smooth with no sign of additional phases on the surfaces. In agreement with the recently reported phase diagram of Valant and Suvorov [16], it was found that the nominally '$Bi_{1.5}MNb_{1.5}O_7$' specimens thereby obtained, while containing a dominant cubic pyrochlore material, were nonetheless clearly not single phase samples. In the case of $M$ = Ni system, the other phases identified were $NiNb_2O_6$ and NiO in agreement with the phase diagram of Valant and Suvorov [16].

New samples were therefore synthesized at a nominal composition of $Bi_{1.67}M_{0.75}Nb_{1.5}O_7$, corresponding to the centre of the cubic pyrochlore solid solution field reported for the $Bi_2O_3$–NiO–$Nb_2O_5$ system by Valant and Suvorov [16] when normalized to seven oxygens. A final annealing temperature of 1100 °C for 3 days was used in the case of $Bi_{1.67}Ni_{0.75}Nb_{1.5}O_7$ (BNN) and 1150 °C for 7 days in the case of $Bi_{1.67}Mg_{0.75}Nb_{1.5}O_7$ (BMN). Both resultant samples appeared single phase using standard two hour Guinier XRD film exposures.

Pressed pellets of these materials were then prepared. The relative densities were 91% for BNN and 94% for BMN, respectively. The pellets were polished and coated with silver paste on both sides, followed by a heat treatment at 550 °C to ensure good electrical contact. The dielectric properties of the pellets were then measured using a high-precision LCR metre (Agilent 4284A).

The average structure unit cell dimension of the samples were determined via X-ray powder diffraction using a Guinier–Hägg camera ($CuK_1$ radiation). High purity Si, NBS #640c, $a$ = 5.431195(9) Å at 22.5 °C was added to the samples to act as an internal standard while the cubic pyrochlore unit cell dimensions were refined using the programme "Unitcell" [19]. Grids suitable for transmission electron microscopy were prepared by crushing the samples in acetone and dispersing them onto lacey carbon coated grids. Electron diffraction patterns (EDPs) were obtained using a Philips EM 430 TEM operating at 300 kV.

Electron probe microanalysis was performed on a JEOL 6400 scanning electron microscope (SEM) equipped with an Oxford Instruments light element EDS detector and Link ISIS SEMquant software. The analyses were carried out at 15 kV and 2 nA using $BiNbO_4$ and NiO or MgO as internal calibration standards.

## 3. Results and discussion

### 3.1. XRD and microanalysis

Careful inspection of heavily exposed Guinier XRD films of the BNN and BMN samples confirmed that the BNN sample was indeed single phase while the BMN sample was found to contain a trace amount of an unknown second phase. In this latter case, four very weak additional lines were observed which could not be indexed

to the BMN cubic pyrochlore phase (see the lines labelled with ** in Table 2). These lines were not visible on the standard 2 h film exposures and only became visible when the X-ray film was exposed for more than 4 h.

The average structure of the cubic pyrochlore BNN and BMN phases were indexed to the usual *Fd*-3*m*, fcc cubic pyrochlore unit cell giving $a = 10.5354(2)$ Å in the case of BNN and $a = 10.5607(5)$ Å in the case of BMN. Two very weak lines (442/006 and 446/028), forbidden for the ideal pyrochlore structure type and indicative of inherent displacive disorder in the O'$A_2$ sub-structure (as pointed out by Vanderah and colleagues [7,8,10]), were observed in both cases (see Tables 1 and 2). The refined lattice parameter for our BNN cubic pyrochlore phase of 10.5354(2) Å differs slightly from the 10.5459(4) Å value reported for the same composition in [16]. In the case of the BMN cubic pyrochlore phase, the refined lattice parameter for our BMN sample of 10.5607(5) Å is quite close to that reported by Sirotinkin and Bush [3] for their nominally $Bi_{1.5}MgNb_{1.5}O_7$, BMN, phase of $a = 10.570(2)$ Å.

In order to confirm the nominal $Bi_{1.67}M_{0.75}Nb_{1.5}O_7$ stoichiometry, the as-synthesized samples were also investigated by EPMA to check for homogeneity and composition, using $BiNbO_4$, NiO or MgO as calibration standards. In the case of BNN, the sample was found to be homogeneous and single phase of average composition $Bi_{1.65(2)}Ni_{0.75(3)}Nb_{1.50(1)}O_7$ (arbitrarily normalized to seven oxygens) i.e. in agreement with the nominal starting stoichiometry within error. The quoted error bars represent the standard deviation of the 40 separate spot analyses used to obtain the quoted average composition. In the case of BMN, the second phase observed in trace quantities in the XRD films was not observed in the SEM. The composition of the dominant cubic pyrochlore phase was found to be somewhat Mg-deficient with average composition $Bi_{1.67(3)}Mg_{0.64(2)}Nb_{1.53(1)}O_7$ (arbitrarily normalized to seven oxygens). The quoted error bars again represent the standard deviation of the 40 separate spot analyses used to obtain the quoted average composition.

### 3.2. Dielectric properties

Fig. 2 shows the measured dielectric permittivities as well as dielectric loss tangents of the above BNN and BMN samples as a function of applied frequency up to 1 MHz at room temperature (a for BNN, b for BMN) as well as their temperature-dependence at 100 kHz and 1 MHz (c for BNN, d for BMN). The largely frequency independent, measured permittivities of BNN and BMN of 116 and 151, respectively, at room temperature are quite high and both ~3–4 times higher than those reported for $Bi_{1.5}NiNb_{1.5}O_7$ and $Bi_{1.5}MgNb_{1.5}O_7$ by Sirotinkin and Bush [3]. Cann et al. [1] reported similar dielectric permittivities (at 1 MHz) of 122 and 210 for $Bi_2(Ni_{2/3}Nb_{4/3})O_7$ and $Bi_2(Mg_{2/3}Nb_{4/3})O_7$,

Table 1
X-ray powder diffraction data for the $Bi_{1.67}Ni_{0.75}Nb_{1.5}O_7$ sample (space group *Fd*-3*m*, #227, $a = 10.5354(2)$ Å)

| No. | *h k l* | $2\theta_{obs}$ | $2\theta_{calc}$ | $\Delta\theta$ | $d_{obs}$ | $I_{obs}$ | Note |
|---|---|---|---|---|---|---|---|
| 1 | 1 1 1 | 14.577 | 14.551 | 0.026 | 6.0719 | 10 | |
| 2 | 0 2 2 | 23.864 | 23.870 | −0.006 | 3.7257 | <1 | |
| 3 | 1 1 3 | 28.079 | 28.068 | 0.011 | 3.1753 | 5 | |
| 4 | 2 2 2 | 29.347 | 29.343 | 0.004 | 3.0409 | 100 | |
| 5 | 0 0 4 | 34.023 | 34.010 | 0.012 | 2.6329 | 50 | |
| 6 | 1 3 3 | 37.176 | 37.168 | 0.008 | 2.4165 | 10 | |
| 7 | 2 2 4 | 41.984 | 41.978 | 0.007 | 2.1502 | <1 | |
| 8 | 1 1 5, 3 3 3 | 44.654 | 44.657 | −0.002 | 2.0276 | 3 | |
| 9 | 0 4 4 | 48.861 | 48.862 | −0.001 | 1.8625 | 570 | |
| 10 | 1 3 5 | 51.268 | 51.259 | 0.009 | 1.7805 | 5 | |
| 11 | 0 0 6, 2 4 4 | 52.030 | 52.040 | −0.010 | 1.7562 | 5 | * |
| 12 | 0 2 6 | 55.091 | 55.086 | 0.005 | 1.6657 | 10 | |
| 13 | 3 3 5 | 57.307 | 57.298 | 0.009 | 1.6064 | <1 | |
| 14 | 2 2 6 | 58.023 | 58.023 | −0.001 | 1.5883 | 50 | |
| 15 | 4 4 4 | 60.871 | 60.869 | 0.002 | 1.5206 | 20 | |
| 16 | 1 1 7, 1 5 5 | 62.956 | 62.952 | 0.004 | 1.4752 | 5 | |
| 17 | 2 4 6 | 66.338 | 66.342 | −0.004 | 1.4079 | <1 | |
| 18 | 1 3 7, 3 5 5 | 68.326 | 68.333 | −0.007 | 1.3717 | 1 | |
| 19 | 0 0 8 | 71.598 | 71.594 | 0.004 | 1.3169 | 20 | |
| 20 | 0 2 8, 4 4 6 | 74.155 | 74.158 | −−0.004 | 1.2777 | <1 | * |
| 21 | 0 6 6, 2 2 8 | 76.688 | 76.690 | −0.002 | 1.2416 | 1 | |
| 22 | 1 5 7, 5 5 5 | 78.572 | 78.572 | 0.000 | 1.2165 | <1 | |
| 23 | 2 6 6 | 79.192 | 79.196 | −0.004 | 1.2086 | 25 | |
| 24 | 0 4 8 | 81.684 | 81.681 | 0.003 | 1.1779 | 25 | |
| 25 | 1 1 9, 3 5 7 | 83.531 | 83.534 | −0.003 | 1.1564 | <1 | |
| 26 | 2 4 8 | 84.139 | 84.150 | −0.011 | 1.1496 | 5 | |
| 27 | 4 6 6 | 86.607 | 86.609 | −0.002 | 1.1231 | 5 | |

*Note*: * Denotes lines forbidden for the ideal pyrochlore structure type and diagnostic of inherent displacive disorder.

Table 2
X-ray powder diffraction data for the $Bi_{1.67}Mg_{0.75}Nb_{1.5}O_7$ sample (space group *Fd*-3*m*, #227, $a = 10.5607(5)$ Å)

| No. | *h k l* | $2\theta_{obs}$ | $2\theta_{calc}$ | $\Delta 2\theta$ | $d_{obs}$ | $I_{obs}$ | Note |
|---|---|---|---|---|---|---|---|
| 1 | 1 1 1 | 14.586 | 14.516 | 0.071 | 6.0679 | 10 | |
| 2 | 0 2 2 | 23.823 | 23.812 | 0.011 | 3.7321 | 3 | |
| 3 | — | 25.322 | — | — | 3.5144 | <1 | ** |
| 4 | 1 1 3 | 27.997 | 27.999 | −0.002 | 3.1844 | 20 | |
| 5 | 2 2 2 | 29.262 | 29.271 | −0.009 | 3.0496 | 100 | |
| 6 | 0 0 4 | 33.923 | 33.927 | −0.004 | 2.6405 | 40 | |
| 7 | 1 3 3 | 37.074 | 37.077 | −0.003 | 2.4230 | 20 | |
| 8 | 2 2 4 | 41.867 | 41.873 | −0.006 | 2.1560 | 1 | |
| 9 | 1 1 5, 3 3 3 | 44.535 | 44.544 | −0.009 | 2.0328 | 10 | |
| 10 | 0 4 4 | 48.736 | 48.738 | −0.002 | 1.8669 | 50 | |
| 11 | — | 48.893 | — | — | 1.8613 | 1 | ** |
| 12 | 1 3 5 | 51.125 | 51.128 | −0.003 | 1.7852 | 5 | |
| 13 | 0 0 6, 2 4 4 | 51.909 | 51.907 | 0.002 | 1.7600 | 1 | |
| 14 | 0 2 6 | 54.949 | 54.944 | 0.006 | 1.6696 | 3 | * |
| 15 | 3 3 5 | 57.155 | 57.149 | 0.006 | 1.6103 | <1 | |
| 16 | 2 2 6 | 57.866 | 57.871 | −0.006 | 1.5922 | 50 | |
| 17 | — | 58.095 | — | — | 1.5865 | <1 | ** |
| 18 | 4 4 4 | 60.720 | 60.708 | 0.012 | 1.5240 | 30 | |
| 19 | 1 1 7, 1 5 5 | 62.791 | 62.785 | 0.007 | 1.4786 | 3 | |
| 20 | 2 4 6 | 66.164 | 66.163 | 0.001 | 1.4112 | <1 | |
| 21 | 1 3 7, 3 5 5 | 68.151 | 68.148 | 0.003 | 1.3748 | <1 | |
| 22 | 0 0 8 | 71.397 | 71.397 | 0.000 | 1.3201 | 20 | * |
| 23 | 0 2 8, 4 4 6 | 73.957 | 73.952 | 0.005 | 1.2806 | <1 | |
| 24 | 1 5 7, 5 5 5 | 78.350 | 78.348 | 0.002 | 1.2194 | 1 | |
| 25 | 2 6 6 | 78.969 | 78.970 | 0.000 | 1.2114 | 25 | |
| 26 | — | 79.243 | — | — | 1.2079 | <1 | ** |
| 27 | 0 4 8 | 81.436 | 81.445 | −0.009 | 1.1808 | 25 | |
| 28 | 1 1 9, 3 5 7 | 83.283 | 83.290 | −0.007 | 1.1593 | 1 | |
| 29 | 2 4 8 | 83.902 | 83.904 | −0.001 | 1.1523 | 5 | |
| 30 | 4 6 6 | 86.345 | 86.351 | −0.006 | 1.1258 | 5 | |

*Note*: *Denotes lines forbidden for the ideal pyrochlore structure type and diagnostic of inherent displacive disorder.
**Denotes four very weak lines belonging to a unknown second phase.

respectively. The measured dielectric loss tangents are also desirably low (e.g. 0.00065 and 0.00042, respectively, at 100 kHz—see Fig. 1(a) and (b)) as are the measured temperature-dependences of the dielectric permittivities (see Fig. 1c and d).

### 3.3. Electron diffraction

Given the crystal chemistry of the underlying average structures of $Bi_{1.65(2)}Ni_{0.75(3)}Nb_{1.50(1)}O_7$, BNN, and $Bi_{1.67(3)}Mg_{0.64(2)}Nb_{1.53(1)}O_7$, BMN (see below), as well as the presence of the diagnostic 006/442 and 028/446 lines in XRD data (see Tables 1 and 2) [7,8,10], it is clear that the O'$A_2$ sub-structures of the BNN and BMN cubic pyrochlores (see Fig. 1) must again be heavily displacively disordered—as seems characteristic of all these Bi-based cubic pyrochlore phases [7,8,10,11,17,18]. From the diffraction point of view, direct evidence as to the nature of this displacive disorder is present in the form of characteristic structured diffuse intensity distributions most easily apparent in electron diffraction data.

Fig. 3 shows (a) $\langle -3,5,0 \rangle$, (b) close to $\langle 2,2,-3 \rangle$ (c) close to $\langle -1,5,0 \rangle$ and (d) close to $\langle 111 \rangle$ zone axis EDPs of the $Bi_{1.65(2)}Ni_{0.75(3)}Nb_{1.50(1)}O_7$, BNN phase while Fig. 4 shows (a) close to $\langle 1,1,-2 \rangle$, (b) close to $\langle 6,-3,-1 \rangle$, (c) close to $\langle -3,3,2 \rangle$ and (b) close to $\langle -1,3,0 \rangle$ zone axis EDPs typical of the $Bi_{1.67(3)}Mg_{0.64(2)}Nb_{1.53(1)}O_7$, BMN, cubic pyrochlore phase. The observed highly structured diffuse distributions in both cases have distinct similarities to the structured diffuse distribution recently shown to be characteristic of a closely related $Bi_{1.89}Fe_{1.16}Nb_{0.95}O_{6.95}$ cubic pyrochlore phase [18] (cf., for example, Fig. 3(b) and (d) with Fig. 3(b) and (d) of [18] and Fig. 4(a) with Fig. 3(a) of [18]). Clearly the structural disorder characteristic of the latter $Bi_{1.89}Fe_{1.16}Nb_{0.95}O_{6.95}$ cubic pyrochlore phase is closely related to that characteristic of the BNN and BMN cubic pyrochlore phases (and, coincidentally, quite dissimilar to that characteristic of BZN and BZN-related cubic pyrochlore phases—cf., e.g. Figs. 3 and 4 with Figs. 3 and 4 of [17]).

In the case of the $Bi_{1.89}Fe_{1.16}Nb_{0.95}O_{6.95}$ cubic pyrochlore phase, the observed structured diffuse distribution took the form of {110}* sheets of diffuse intensity perpendicular to each of the six $\langle 110 \rangle$ directions of real space giving rise to diffuse streaking along all $\mathbf{G} \pm \varepsilon \langle h,-h,l \rangle^*$, $\mathbf{G}$ an average structure Bragg reflection and $\varepsilon$ continuous, directions of reciprocal space. Very similar $\mathbf{G} \pm \varepsilon \langle h,-h,l \rangle^*$ diffuse streaking is also apparent in Figs. 3

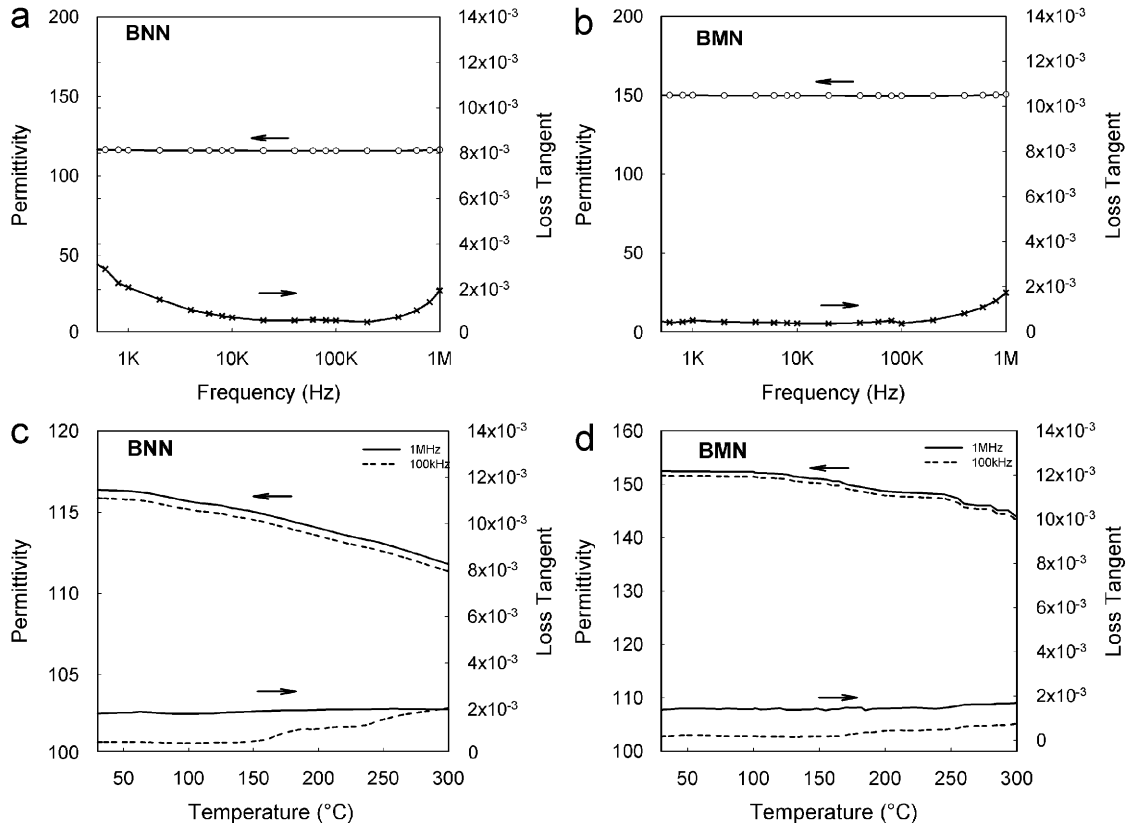


Fig. 2. The measured dielectric permittivities as well as dielectric loss tangents of the BNN and BMN samples as a function of applied frequency up to 1 MHz at room temperature (a for BNN, b for BMN) as well as their temperature-dependence at 100 kHz and 1 MHz (c for BNN, d for BMN).

and 4, e.g. along the $\mathbf{G}\pm\varepsilon\langle 10,-4,4\rangle^*$, $\mathbf{G}\pm\varepsilon\langle -4,10,4\rangle^*$ and $\mathbf{G}\pm\varepsilon\langle 668\rangle^*$ lines of reciprocal space in Fig. 3(b) or along the $\mathbf{G}\pm\varepsilon\langle 3,-1,1\rangle^*$, $\mathbf{G}\pm\varepsilon\langle 1,-3,-1\rangle^*$ and $\mathbf{G}\pm\varepsilon\langle 668\rangle^*$ directions of reciprocal space in Fig. 4(a) etc. As discussed in [18], there are characteristic 'extinction conditions' associated with this diffuse streaking, e.g. the $\mathbf{G}\pm\varepsilon\langle 668\rangle^*$ diffuse streaking in Fig. 3(b) runs through the $[hkl]^*$, $h-k=4J$, $J$ an integer, parent Bragg reflections such as, e.g. $[6,-6,0]^*$ but not through Bragg reflections such as $[424]^*$, etc. Such 'extinction conditions' along with the $\{110\}^*$ sheet form of the diffuse distribution are characteristic of essentially independent $\beta$-cristobalite-like tetrahedral edge rotation of the O'$A_2$ sub-structure of the ideal pyrochlore structure type (as shown in Fig. 5). Clearly similar displacive modulations of the O'$A_2$ sub-structure must also be taking place in both BNN and BMN.

While the EDPs shown in Figs. 3 and 4 are quite similar to those shown in [18], however, there are nonetheless also some noticeable differences—in particular, the linear $\mathbf{G}\pm\varepsilon\langle h,-h,l\rangle^*$ streaking that exists at the orientations discussed above seem to break up into curved arcs at other orientations (see, for example, Figs. 3(a) and (c) in the case of BNN and Fig. 4(d) in the case of BMN). In the case of the $\mathbf{G}\pm\varepsilon\langle 535\rangle^*$ 'streak' (labelled with a white line) which should run through the $\mathbf{G}=[0,0,-8]^*$ Bragg reflection in Fig. 3(a), for example, it is clear that this is no longer a continuous streak but has rather broken up into curved segments that almost look like they are part of an essentially continuous diffuse circle centred on $[0,0,-4]^*$ (see the white circle in Fig. 3a).

The significance of this is far from clear to the authors. One possibility is that the presence of significant numbers of vacancies on the $A$ site (implied by the stoichiometry of these BNN and BMN phases) may mean that the initially independent $\beta$-cristobalite-like tetrahedral edge rotations of the O'$A_2$ sub-structure shown in Fig. 5 are now somehow coupled together leading to a related but rather more complex diffuse scattering distribution than $\{110\}^*$ sheets of diffuse intensity perpendicular to each of the six $\langle 110\rangle$ directions of real space. To make further progress, however, requires not only an understanding of the local crystal chemistry of the underlying average structures but would also require full scale Monte Carlo modelling of an appropriately disordered O'$A_2$ sub-structure, well beyond the scope of the current contribution.

### 3.4. Crystal chemical considerations

In order to obtain insight into the local forces responsible for the structured diffuse scattering shown in Figs. 3 and 4, an understanding of the local crystal chemistry of the underlying *Fd*-3*m* average structures of the $Bi_{1.65}Ni_{0.75}Nb_{1.50}O_7$, BNN, and $Bi_{1.67}Mg_{0.64}Nb_{1.53}O_7$, BMN, cubic pyrochlore phases is an indispensible first

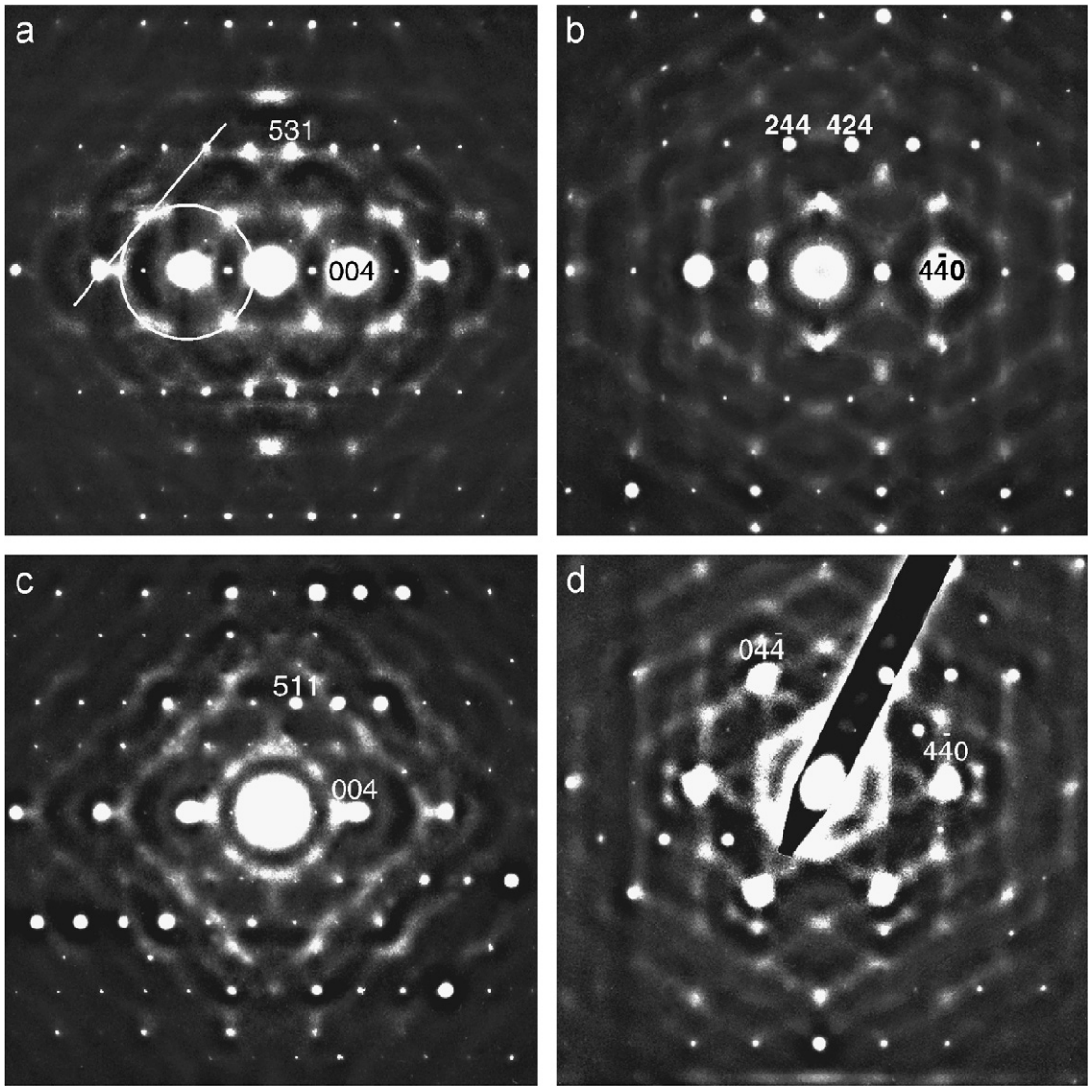


Fig. 3. (a) ⟨−3,5,0⟩, (b) close to ⟨2,2,−3⟩ (c) close to ⟨−1,5,0⟩ and (d) close to ⟨111⟩ zone axis EDPs of the $Bi_{1.65(2)}Ni_{0.75(3)}Nb_{1.50(1)}O_7$, BNN, cubic pyrochlore. Note the highly structured, characteristic diffuse intensity distribution accompanying the Bragg reflections of the underlying pyrochlore type average structure.

step. For this purpose, it is assumed that the $B$ sites of the ideal pyrochlore $A_2B_2O(1)_6O(2)_1$, or $B_2O(1)_6 \cdot O(2)A_2$, structure type ($A$ on 16$d$ at 1/2, 1/2, 1/2; $B$ on 16$c$ at 0, 0, 0; O(1) on 48$f$ at $x$, 1/8, 1/8 and O(2) on 8$b$ at 3/8, 3/8, 3/8; origin setting 2; see Fig. 1) are fully occupied. The stoichiometry of the BNN cubic pyrochlore is thus written in the form $(Bi_{0.825}Ni_{0.125}\square_{0.05})_2(Ni_{0.25}Nb_{0.75})_2O_7$ while that of the BMN cubic pyrochlore is written in the form $(Bi_{0.835}Mg_{0.085}\square_{0.08})_2(Mg_{0.235}Nb_{0.765})_2O_7$, where the symbol $\square$ represents a vacancy on the ideal pyrochlore $A$ site.

The one unknown fractional co-ordinate in the ideal pyrochlore structure type, the $x$ fractional co-ordinate of O(1), can be readily estimated using the bond valence sum approach (see also [11,17,18]) and the $R_0$ parameters listed in [20]. Given the average occupancies of the $B$ sites, the expected average $B$–O bond length, $R(B\text{–O})$ should be such that:

$$\begin{aligned} \mathrm{AV}(B) &= 6 \times 0.25 \exp\{^{(1.654-R)}/0.37\} \\ &\quad + 6 \times 0.75 \exp\{^{(1.911-R)}/0.37\} \\ &= 1/4 \times 2 + 3/4 \times 5 = 4.250 \end{aligned}$$

and

$$\begin{aligned} \mathrm{AV}(B) &= 6 \times 0.235 \times \exp\{^{(1.693-R)}/0.37\} \\ &\quad + 6 \times 0.765 \exp\{(1.911 - R)/0.37\} \\ &= 0.235 \times 2 + 0.765 \times 5 = 4.295, \end{aligned}$$

in the cases of BNN and BMN, respectively. (Note AV in the above equation refers to the so-called apparent valence or bond valence sum [20].) This occurs for $R = 1.9891$ Å in the case of BNN and 1.9938 Å in the case of BMN. An average $R(B\text{–O})$ bond length of 1.9891 Å occurs for

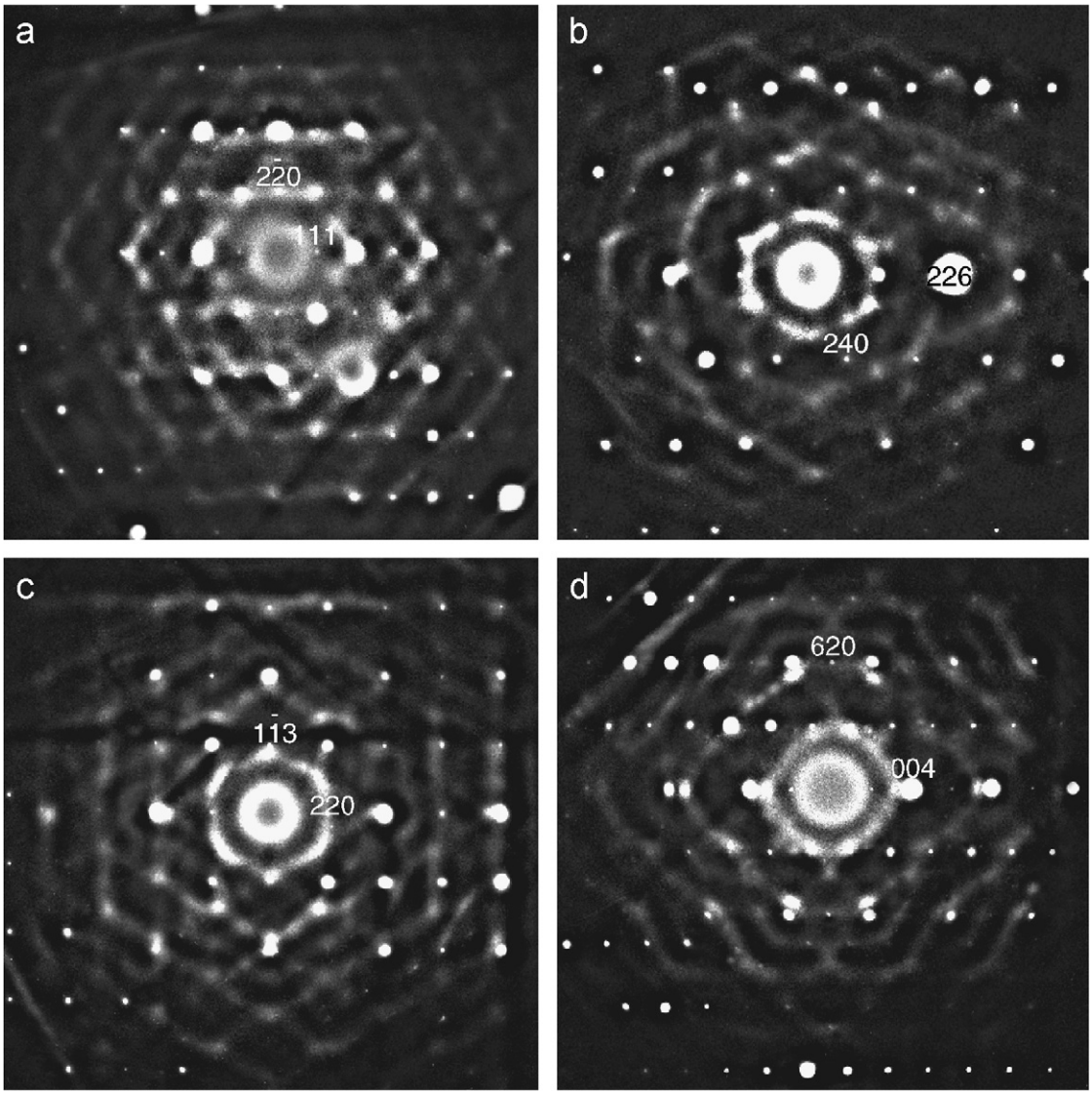


Fig. 4. (a) Close to ⟨1,1,−2⟩; (b) close to ⟨6,−3,−1⟩; (c) close to ⟨−3,3,2⟩; and (b) close to ⟨−1,3,0⟩ zone axis EDPs of the $Bi_{1.67(3)}Mg_{0.64(2)}Nb_{1.53(1)}O_7$, BMN, cubic pyrochlore.

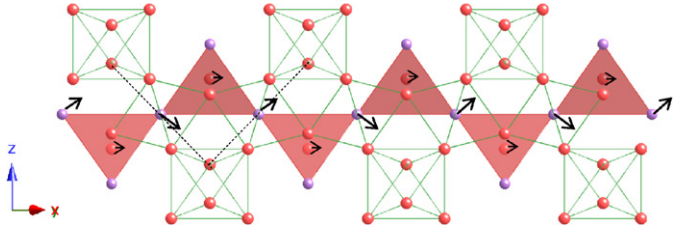


Fig. 5. The characteristic 1-D, $\beta$-cristobalite type displacive disorder of the O'$A_2$ sub-structure drawn relative to the surrounding $B_2O_6$ octahedral framework sub-structure. The tetrahedral edge rotation axes run along the projection direction.

$x = 0.3163$ given the relation between $R(B\text{–O}) = \sqrt{\{(x-1/4)^2 + 2(1/8)^2\}} \times 10.5354\,\text{Å}$ and $x$. Likewise, an average $R(B\text{–O})$ bond length of 1.9938 Å occurs for $x = 0.3163$ given $a = 10.5607\,\text{Å}$ for BMN. The bond valence sum prediction for the value of $x$ is thus ~0.3163 for both BNN and BMN.

With this choice of $x$, the 'average' $B$ cations are reasonably happily bonded in the average pyrochlore structure (see Tables 3 and 4), particularly given that additional small amplitude relaxations of the O(1) array (away from the $Ni^{2+}/Mg^{2+}$ ions and towards the $Nb^{5+}$ ions) associated with the local distribution of $Nb^{5+}$ and $Ni^{2+}/Mg^{2+}$ on the $B$ sites can be expected to simultaneously reduce the initial overbonding of the $Ni^{2+}/Mg^{2+}$ ions and underbonding of the $Nb^{5+}$ ions. (For $Nb^{5+}$ in the $B$ site, the ideal $B$–O distance $R$(Nb–O) is given by that distance which corresponds to an AV [20] of 5/6). From [20], this distance is given by $1.911–0.37\ln(5/6) = 1.9785$ Å. For $Ni^{2+}/Mg^{2+}$ in the same $B$ site, the equivalent ideal $B$–O distance $R(\text{Ni/Mg–O}) = 1.654/1.693–0.37\ln(2/6) = 2.0605/2.0995$ Å, respectively). Note, however, that both the $Bi^{3+}$ and $Ni^{2+}/Mg^{2+}$ ions are significantly under-bonded in the ideal pyrochlore $A$ site, particularly the latter $Ni^{2+}/Mg^{2+}$ ions which are

Table 3
Bond valence sums (AVs) for the cubic pyrochlore average structure of BNN

| *A* | *B* | AV(*A*) | AV(*B*) | AV(O1) | AV(O2) |
|---|---|---|---|---|---|
| Bi | Nb | 2.392 | 4.858 | 2.019 | 2.387 |
| Bi | Ni | 2.392 | 2.426 | 1.208 | 2.387 |
| Ni | Nb | 0.736 | 4.858 | 1.742 | 0.735 |
| Ni | Ni | 0.736 | 2.426 | 0.932 | 0.735 |

Table 4
Bond valence sums (AVs) for the cubic pyrochlore average structure of BMN

| *A* | *B* | AV(*A*) | AV(*B*) | AV(O1) | AV(O2) |
|---|---|---|---|---|---|
| Bi | Nb | 2.354 | 4.796 | 1.991 | 2.352 |
| Bi | Mg | 2.354 | 2.661 | 1.280 | 2.352 |
| Mg | Nb | 0.805 | 4.796 | 1.733 | 0.804 |
| Mg | Mg | 0.805 | 2.661 | 1.021 | 0.804 |

under-bonded by a massive 63/60%, respectively. This massive under-bonding of the $Ni^{2+}/Mg^{2+}$ ions is the reason why the latter $Ni^{2+}/Mg^{2+}$ ions are conventionally considered to be too small to occupy the pyrochlore *A* sites.

Now consider the second O(2)$A_2$ tetrahedral corner-connected substructure of anti-cristobalite structure type (see Fig. 1). The O(2) anion in this sub-structure is tetrahedrally co-ordinated by 4 *A* cations at an average distance $R(O'–A) = (\sqrt{3}/8)a = 2.2810/2.2865$ Å determined solely by the cubic lattice parameter *a*. The introduction of □'s onto the *A* sites to accompany the majority $Bi^{3+}$ and minority $Ni^{2+}/Mg^{2+}$ cations considerably complicates the local crystal chemistry, not only because it creates a much wider range of potential local [$A_4$] stoichiometries but also because their presence or otherwise significantly affects the AV of the O(2) anions which it neighbours and hence the driving forces for local displacive disorder of the $Bi^{3+}$ and minority $Ni^{2+}/Mg^{2+}$ cations.

Tables 5 and 6 list the calculated AV of a centreing O(2) anion depending upon the local [$A_4$] stoichiometry of the tetrahedron of cations surrounding it. The probability of that particular configuration (Prob. P) occurring (under the unlikely assumption of random ordering of the $Bi^{3+}$, $Ni^{2+}/Mg^{2+}$ and □'s on the ideal pyrochlore *A* site) is also given. While not all theoretically possible local [$A_4$] stoichiometries are listed (only those with two Bi ions or more are listed), those that are listed account for over 98% of those theoretically possible. For the most likely [$Bi_4$] or [$Bi_3M$] configurations (~70%) it can be seen that the centreing O(2) anion is either happily bonded or over-bonded in both cases implying that the heavily under-bonded $Bi^{3+}$ and $Ni^{2+}/Mg^{2+}$ cations cannot significantly increase their AV, i.e. improve their under-bonding, by moving closer to the O(2) anions but must instead move off-centre perpendicular to the local O(2)−*A*–O(2) axis, as is ensured by the *β*-cristobalite-type displacive distortion

Table 5
AVs for O(2) dependent upon local [$A_4$] stoichiometry for BNN

| | [$Bi_4$] | [$Bi_3Ni$] | [$Bi_3$] | [$Bi_2Ni_2$] | [$Bi_2Ni_1□_1$] | [$Bi_2□_2$] |
|---|---|---|---|---|---|---|
| AV{O(2)}[$A_4$] | 2.387 | 2.071 | 1.790 | 1.559 | 1.376 | 1.194 |
| Prob. *P* | 0.463 | 0.281 | 0.112 | 0.064 | 0.051 | 0.010 |

Table 6
AV's for O(2) dependent upon local [$A_4$] stoichiometry for BMN

| | [$Bi_4$] | [$Bi_3Mg$] | [$Bi_3□$] | [$Bi_2Mg_2$] | [$Bi_2Mg_1□_1$] | [$Bi_2□_2$] |
|---|---|---|---|---|---|---|
| AV{O(2)}[$A_4$] | 2.352 | 1.965 | 1.764 | 1.578 | 1.377 | 1.176 |
| Prob. *P* | 0.486 | 0.198 | 0.186 | 0.030 | 0.057 | 0.027 |

shown in Fig. 5 and implied by the structured diffuse scattering apparent in Figs. 3(b), (d) and 4(a).

When either a single □ or more than one non-Bi ion is present in the local [$A_4$] configuration, however, the O(2) anion becomes significantly under-bonded, presumably allowing it to move directly towards any neighbouring also under-bonded *A* cations thus improving the bond valence sum requirements of all ions involved. The presence of a significant concentration of □'s on the *A* sites of these "…misplaced-displacive cubic pyrochlore…" phases [7] thus would seem to introduce extra flexibility as well as complexity into the local crystal chemistry.

Now consider the [$A_2B_2$] co-ordination environment of the O(1) ions. Tables 7 and 8 list the calculated AV of a centreing O(1) anion depending upon the local [$A_2B_2$] stoichiometry of the tetrahedron of cations surrounding it. The probability of that particular configuration occurring (under the unlikely assumption of random ordering) is also given. While again not all theoretically possible local [$A_2B_2$] stoichiometries are listed (only those with at least one Bi occupying an *A* site are listed), those that are listed account for over 90% of those theoretically possible. It can be seen that the AV of an O(1) ion depends most significantly on the identity of the two *B* site cations to which it is bonded, being significantly under-bonded if one or other of these two *B* sites is occupied by a $Ni^{2+}/Mg^{2+}$ cation and essentially happily bonded if both are occupied by a $Nb^{5+}$ cation.

Given that the drastically under-bonded *A* site cations, in the majority of cases, must move off-centre away from the local O(2)–*A*–O(2) axis towards some (but simultaneously away from other) O(1) ions, it would seem to make most crystal chemical sense for them to move away from the O(1) ions that are bonded to 2 Nb *B* site cations and towards those that are bonded to 1 Nb and one $Ni^{2+}/Mg^{2+}$ cation. Bond valence sum considerations suggest that a transverse shift of the *A* cation of ~0.65 Å in the case of $Bi_{1.65}Ni_{0.75}Nb_{1.50}O_7$ can increase the AV of the initially under-bonded Bi ion from 2.39 to 3.05. The equivalent effect in the case where *A* = Ni is, however, much more modest with the Ni AV only increasing from 0.74 to 0.94! It seems that such a large amplitude transverse displacement of the *A* cation is not the way to significantly improve the

Table 7
AV's for O(1) dependent upon local $[A_2B_2]$ stoichiometry for BNN

| | $[Bi_2Nb_2]$ | $[Bi_2NbNi]$ | $[BiNiNb_2]$ | [BiNiNbNi] | $[Bi\square Nb_2]$ | $[Bi\square NbNi]$ |
|---|---|---|---|---|---|---|
| AV{O(1)}$[A_2B_2]$ | 2.019 | 1.614 | 1.881 | 1.475 | 1.819 | 1.414 |
| Prob. $P$ | 0.383 | 0.255 | 0.116 | 0.077 | 0.046 | 0.031 |

Table 8
AV's for O(1) dependent upon local $[A_2B_2]$ stoichiometry for BMN

| | $[Bi_2Nb_2]$ | $[Bi_2NbMg]$ | $[BiMgNb_2]$ | [BiMgNbMg] | $[Bi\square Nb_2]$ | $[Bi\square NbMg]$ |
|---|---|---|---|---|---|---|
| AV{O(1)}$[A_2B_2]$ | 1.991 | 1.635 | 1.862 | 1.506 | 1.795 | 1.439 |
| Prob. $P$ | 0.408 | 0.251 | 0.083 | 0.051 | 0.078 | 0.048 |

drastic under-bonding of the $Ni^{2+}/Mg^{2+}$ cations in these structures. Following [17], it is suggested that the only way to significantly improve the drastic under-bonding of the $Ni^{2+}/Mg^{2+}$ cations in these materials is for the two O(2) anions bonded to it to both significantly contract in towards the $Ni^{2+}/Mg^{2+}$ cation.

The question of how to put all of the above local crystal considerations together into a truly coherent as well as understandable model of the local crystal chemistry and resultant displacive distortions of this remarkable family of materials is clearly a distinctly non-trivial problem and remains an important future challenge. It nonetheless seems clear that the small but significant $\square$ concentration on the $A$ sites of these "…misplaced-displacive cubic pyrochlore …" phases [7] is a very important parameter and plays a crucial role as regards the local crystal chemistry and resultant local displacive distortions.

## Acknowledgments

BN, YL and RLW acknowledge financial support from the Australian Research Council (ARC) in the form of an ARC Discovery Grant.

## References

[1] D.P. Cann, C.A. Randall, T.R. Shrout, Solid State Commun. 100 (1996) 9529–9534.
[2] X. Wang, H. Wang, X. Yao, J. Am. Ceram. Soc. 80 (1997) 2745–2748.
[3] V.P. Sirotinkin, A.A. Bush, Inorg. Mater. 39 (2003) 974–977.
[4] M. Valant, P.K. Davies, J. Am. Ceram. Soc. 83 (2000) 147–153.
[5] W. Ren, S. Trolier-McKinstry, C.A. Randall, T.R. Shrout, J. Appl. Phys. 89 (2001) 767–774.
[6] J. Lu, S. Stemmer, Appl. Phys. Lett. 83 (2003) 2411–2413.
[7] T.A. Vanderah, I. Levin, M.W. Lufaso, Eur. J. Inorg. Chem. (2005) 2895–2901.
[8] T.A. Vanderah, T. Siegrist, M.W. Lufaso, M.C. Yeager, R.S. Roth, J.C. Nino, S. Yates, Eur. J. Inorg. Chem. (2006) 4908–4914.
[9] K.B. Tan, C.K. Lee, Z. Zainal, G.C. Miles, A.R. West, J. Mater. Chem. 15 (2005) 3501–3506.
[10] I. Levin, T.G. Amos, J.C. Nino, T.A. Vanderah, C.A. Randall, M.T. Lanagan, J. Solid State Chem. 168 (2002) 69–75.
[11] R.L. Withers, T.R. Welberry, A.-K. Larsson, Y. Liu, L. Norén, H. Ründlof, F.J. Brink, J. Solid State Chem. 177 (2004) 231–244.
[12] H. Du, X. Yao, L. Zhang, Ceram. Int. 28 (2002) 231–234.
[13] J.Y. Kim, D.W. Kim, H.S. Jung, K.S. Jung, Jpn. J. Appl. Phys. 44A (2005) 6648–6653.
[14] M. Valant, P.K. Davies, J. Mater. Sci. 34 (1999) 5437–5442.
[15] H. Du, X. Yao, J. Mater. Sci.: Mater. Electron. 15 (2004) 613–616.
[16] M. Valant, D. Suvorov, J. Am. Ceram. Soc. 88 (2005) 2540–2543.
[17] Y. Liu, R.L. Withers, T.R. Welberry, Hong Wang, Huiling Du, J. Solid State Chem. 179 (2006) 2141–2149.
[18] W. Somphon, V. Ting, Y. Liu, R.L. Withers, Q. Zhou, B.J. Kennedy, J. Solid State Chem. 179 (2006) 2495–2505.
[19] B. Noläng, Inst. Materialkemi, Ångströmlaboratoriet, Box 538, SE-751 21 Uppsala, Sweden.
[20] N.E. Brese, M. O'Keeffe, Acta Crystallogr. B 47 (1991) 192–197.